Characterization method for mass mixing in batch reactors based on temperature profiles

Characterization method for mass mixing in batch reactors based on temperature profiles

Lennart Camps[a], Luc Moens[b], Urs Groth[c], Leen Braeken[a,d], Simon Kuhn[d], Leen C.J. Thomassen[a,d]*

[a]KU Leuven, Faculty of engineering technology, Lab4U; Agoralaan building B box 8, 3590 Diepenbeek BELGIUM

[b]Janssen Pharmaceutica, Turnhoutseweg 30, 2430 Beerse BELGIUM

[c]Mettler Toledo GmbH, Heuwinkelstrasse 3, 8606 Nänikon SWITZERLAND

[d]KU Leuven, Department of Chemical engineering, Celestijnenlaan 200F, 3001 Leuven BELGIUM

ABSTRACT. Measuring mass mixing in batch reactors is of great interest to prevent yield losses during scale-up of reactions. In this work, we present a novel tool to accomplish this: the heat pulse method. This is a thermal-based technique consisting of a local heat pulse, applied electrically or by a hot liquid injection, during 10 seconds at a power of 5 to 15 W and subsequent measurement of temperature increase at locations of interest. The 95% mixing time from corrected and smoothed temperature profile characterizes heat mixing. A heat mixing model identifies the contributions of thermal conduction and convection and hereby relates local heat and mass mixing in a 800 mL in

a 1L batch reactor with a 45° 4 blade downward pitched turbine. The heat pulse method is applicable on different reactors, solvent independent and non-destructive. Experiments are repeatable and mixing at reactive circumstances can be mimicked.

KEYWORDS. heat pulse method, micromixing time, batch reactor, mixing scales, heat and mass mixing.

1. Introduction

Inefficient scale-up of mixing-sensitive reactions, where the mixing efficiency of the industrial scale does not correspond with the lab scale, generally leads to a loss of yield of 5% in reactors, which causes a loss up to 10 billion dollars each year in America alone[1]. Scale-up from lab scale to industrial scale is a crucial step to industrial production but not straight forward as the increase in scale influences both mass and heat transfer in a reactor[1–4]. Slow mass transfer, which consists of convection and diffusion, during scale-up leads to a decreased supply of reagents limiting the global reaction rate and conversion[5]. To prevent slow mass transfer, a better understanding of mixing and the mixing mechanisms is required[1,6,7].

1.1 Mass mixing mechanisms

For mass mixing, the added reagent gets distributed on a macro scale first. Convection is the main macromixing mechanism at which the added stirrer energy causes engulfment and hereby the mass is mixed on the largest scale over the reactor content[1]. The swirls and eddies from the engulfment, due to the stirrer energy, continue to mix the reagent to smaller scales, to the meso scale and finally to the microscopic scale. At this scale, mixing of the reagents by stirrer energy does not proceed as fast and efficiently anymore. From this scale, diffusion is the dominant mixing mechanism and causes the reagents to collide with each other and react[1,8–15].

Micromixing time, which is based on the Kolmogorov theory, is used as a characteristic value for mass mixing (convection). The micromixing time represents the mixing time by engulfment from macroscopic scale to the microscopic scale[1,8,11]. The corresponding equation for the average micromixing time in a batch reactor is shown in eq 1. The equation is only valid at Schmidt numbers below 4000. The Schmidt number represents the ratio between momentum diffusivity and mass diffusivity[10,11,13,14].

$$t_{m,ave} = 17.2 * \sqrt{\frac{\nu}{\varepsilon_{ave}}} = 17.2 * \sqrt{\frac{\frac{\mu}{\rho}}{\frac{n_p * N^3 * D^5}{V}}} \quad (1)$$

With $t_{m,ave}$ the average micromixing time, ν the kinematic viscosity, ε_{ave} the average energy dissipation, μ the dynamic viscosity, n_p the power number, N the rotational speed, D the impeller diameter and V the volume. Calculation of the power number in the reactor is based on the equations of Furukawa *et al*[16]. While eq 1 takes the average micromixing time into account, it should be noted that the mixing efficiency in batch reactors varies strongly between different locations. In order to compare average micromixing time and local micromixing time, shown in eq 3, a local mixing factor, f_{local}, should be taken into account, which is the ratio between the local energy dissipation, ε_{local}, and the average energy dissipation, ε_{ave}, shown in eq 2[17].

$$f_{local} = \frac{\varepsilon_{local}}{\varepsilon_{ave}} \quad (2)$$

$$t_{m,local} = 17.2 * \sqrt{\frac{\nu}{\varepsilon_{ave}}} * f_{local}^{-\frac{1}{2}} \quad (3)$$

1.2 Heat mixing mechanisms

Heat and mass mixing are different and these differences have to be taken into account: the heat mixing routes are convection (equivalent to mass transfer by convection), complemented by thermal radiation and thermal conduction[18–20]. Thermal radiation has a negligible influence on temperatures below 100°C (Stefan-Boltzmann formula)[18,21], but thermal conduction plays an

important role. However, at a constant temperature and in a single solvent, thermal conduction remains the same, which makes it possible to measure and study the influence of convection (mass mixing). The thermal diffusivity (α), a solvent characteristic, is used as a characteristic value for the thermal conduction. This signifies the rate of heat transfer via thermal conduction in a material applying a temperature gradient, shown in eq 4[1,18,19].

$$\alpha = \frac{k}{\rho * c_p} \quad (4)$$

With k the thermal conductivity, ρ the density and c_p the heat capacity. In contrast to mass mixing, the mechanisms and their corresponding mixing scales are harder to explain for heat mixing: thermal convection is still present, mainly acting on the macro and meso scale, whereas thermal conduction is the dominant mechanism on the microscopic scale. However, the contribution of conduction on the meso and macro scale compared to convection is less known. Thermal conduction is a mechanism, similar to diffusion for mass mixing. However, the former mechanism is faster, causing an increasing influence on the larger mixing scales[18–21]. In conclusion, the relation between heat and mass mixing needs a better understanding and is studied upon introducing heat pulses in a reactor.

1.3 Mixing characterization methods

For a stirred batch reactor, the physical quantity 'mixing time' is mainly used to characterize mixing[6,22–25]. A 95% mixing time signifies the time after which the volume has obtained a level of 95% homogeneity after an initially inhomogeneous mixture[1,22,23,25–27]. Methods that are able to measure mass mixing in batch reactors can be divided in two main groups: global and local methods. Each main group consists of two sub groups: mathematical and experimental methods for global measurements and physical and chemical methods for local measurements[23,28]. Table 1 shows a summary of the different approaches of mass mixing characterization.

Table 1. Advantages and drawbacks of different methods of mass mixing characterization

	GLOBAL		LOCAL	
Method	MATHEMATICAL	EXPERIMENTAL	PHYSICAL	CHEMICAL
Example	• Computational fluid dynamics (CFD) [29]	• Colorization[1,22,28] • Electrical resistance tomography[1,23,28]	• Conductometry[23,28] • pH[22,26,28]	• Iodide-iodate[1,30,31] • Diazo coupling[32,33]
Advantage	+ No waste[29] + Identify dead zones[29] + Scale-up predictions[29] + Reaction mixtures[29]	+ Identify dead zones[23,28] + Non-intrusive[23,28]	+ Accurate[23,28] + In situ[23,28] + Scale-up predictions[23]	+ In situ[31,32] + Reaction based[31,32]
Drawbacks	– Assumptions[29] – Theoretical[29]	– Transparent vessels[22,29] – 2D measurement of 3D mixing process[22,28] – Designated solvent[28]	– Solvent destructive[23,28,29] – Difficulty to measure dead zones[23,28,29] – Designated solvent[23,28,29] – No end point of mixing in whole tank[23,28,29]	– Designated solvent[31,32] – Difficult reaction kinetics and experimental variability[31,32] – Safety[11,31,32]

1.3.1 Global mathematical methods. Global methods measure mass mixing over the entire reactor volume, mostly ex situ[1,6,11,34]. The first, group are simulation programs, which often use

computational fluid dynamics. The mathematical method uses assumptions in order to simulate the reality. This results in the need for a parameter optimization and experimental validation at each scale[1–5]. For example, a simulation with Dynochem performed by Deans *et al*. in a lab reactor of 0.5 L has a deviation of 29% on the 95% mixing time compared to the experimental test with decolorization[7]. Stoker compares a CFD scale-up with constant power per volume with experimental tests[6]. At the 3 L scale differences between CFD and experiments occur: CFD predicts a 95% mixing time of 13 s while experimental tests indicate a 95% mixing time of 9 s. However, at the 2000 L scale the differences enlarge: CFD predicts a 95% mixing time of 91 s, while experimental tests result in a 95% mixing time of 31 s[6].

1.3.2 Global experimental methods. The second group of global mass mixing measurement methods are the experimental methods, whereby mass mixing is measured by injecting a tracer and monitoring the entire reactor volume. The global experimental methods are non-intrusive, able to identify dead zones, segregated regions and mixing patterns and indicate the end point of mixing. However, they are often inaccurate since it is difficult to make a 3D visualization of the external (2D) measurement. Electrical resistance tomography (ERT) measures conductivities at the outside of the reactor, which can produce cross-sectional (2D) images when processed with algorithms. Multiple cross-sectional images at different heights determine flow patterns over the reactor (3D). This non-intrusive technique is able to accurately measure mass mixing in reactors, however, the technique is expensive and more complicated due to the need of data processing algorithms.

Colorization injects a dye as tracer or a reagent, which causes a coloring chemical reaction, while the camera records mixing in the total reactor volume. The study of Deans *et al*. uses on the one hand a phenolphthalein decolorization by acid injection, while on the other hand a methylene blue

dye injection colorization is performed. The average 95% mixing time of the first method is 39% lower than the 95% mixing time of the second method in the 500ml reactor at 80 RPM. The difference between the two techniques is caused by the injection of the highly concentrated sulfuric acid versus a low concentrated methylene blue solution. The concentrated sulfuric acid has a higher density than water and therefore sinks to the bottom of the reactor, ultimately resulting in different 95% mixing times. This indicates that the method is not straightforward and small changes in the methods create big differences in mixing times, especially at relatively low rotational speeds. Additionally, transparent vessels are required for colorization, which is commonly not achievable for industrial application making it unsuitable for scale-up[6,7,12,22,23,29,35].

1.3.3 Local chemical methods. Local methods use in situ probes at the location of interest: these methods use physical or chemical methods to determine mass mixing at a specific location in the reactor. By measuring at multiple locations or using multiple probes, the reactor can be characterized. Local chemical methods use a mixing sensitive reaction, where the yield determines the degree of mass mixing in the reactor. A reaction limiting reagent is added and the yield of the reaction characterizes mass mixing at the location of injection. Local chemical methods are able to characterize mass mixing at a position in the reactors with a designated solvent, but are very complex to use for scale-up, the used chemicals can cause safety issues and reproducibility is rather low. Therefore, chemical local methods are more interesting to investigate the influence of certain reactor parameters (stirrer type, speed, presence of a baffle,…) in the same reactor[1,12,36,37].

1.3.4 Local physical methods. Local physical measurements add a tracer at one location, while a probe measures a value of mass mixing at a different location. Similar to the pH method, where an injection of a reagent causes a sudden change in pH and a pH sensor measures the change in pH, the conductivity method adds a salt solution as a tracer, while a conductivity probe measures

the change in conductivity at a different location. Local physical methods have as advantages that they are accurate, measure in situ and can be used in industrial volumes. Their disadvantages are the destruction of the solvent, the limitation to a designated solvent and their solvent properties and the difficulty of measuring dead zones, segregated regions or the end point of mixing[6,12,22,23,25,29,38].

1.4 Heat pulse method.

None of the available methods are applicable in any solvent or non-reactive mixture on multiple scales nor are the measurement probes small enough in order to measure at multiple locations in lab scale reactors. Mass mixing characterization of different solvents or non-reactive mixtures are of great interest since it mimics the mixing conditions of the reaction. Measurements at multiple locations provide more information on the mixing pattern, end point of mixing in the reactor and mass mixing homogeneity of the reactor volume while the use of the method on multiple scales enables scale-up of mixing by experimental correlations[29].

This paper presents a novel measurement method, that addresses these issues and tackles scale-up problems. The goal of this new, local method is to achieve a better characterization of mass mixing in batch reactors. The method has to be able to characterize mass mixing of non-reactive mixtures in an accurate, fast, reproducible way without destruction of the reactor content. This new thermal-based method, called “The heat pulse method” consists of a small amount of heat which is applied to the reactor content, electrically or by a hot liquid injection, at one location, while temperature sensors record the temperature profile at different locations in the reactor. The 95% mixing time from the heat pulse method depends on heat mixing, where thermal diffusivity represents the thermal conduction and micromixing time the convection. These characteristics are

investigated in order to be able to study the influence of each mechanism on heat mixing and thus in order to be able to use the heat pulse method to measure mass mixing.

2. Materials and Methods

2.1 Reactor set-up

The automated calorimetric lab reactor OptiMax of Mettler Toledo is used for the experiments. All experiments in this study are performed with a 1 L unbaffled reactor with 800 mL solvent, set at 20.00 °C, with a 45° downward 4 pitched blade turbine (4PBT). Figure 1 shows that the injection is close to the stirrer. At these conditions, micro and macromixing are similar or better than a baffled tank at lab scale[39]. The reactor set-up with stirrer, injection probe and measurement probes is shown in Figure 1. In order to accurately measure the temperature profile that corresponds to the launched heat of the injection probe, the experiments are performed at isoperibolic conditions. These conditions are fulfilled when the jacket of the reactor has a constant temperature. The constant jacket temperature is set to a defined temperature in order to prevent net heat exchange between the environment and the reactor volume[40–42]. However, the small temperature increase of approximately 0.05 °C, still causes some heat losses. For example, the heat losses of the heat pulse (10 W for 10 s) in 800 mL of water stirred at 100 RPM are 5%.

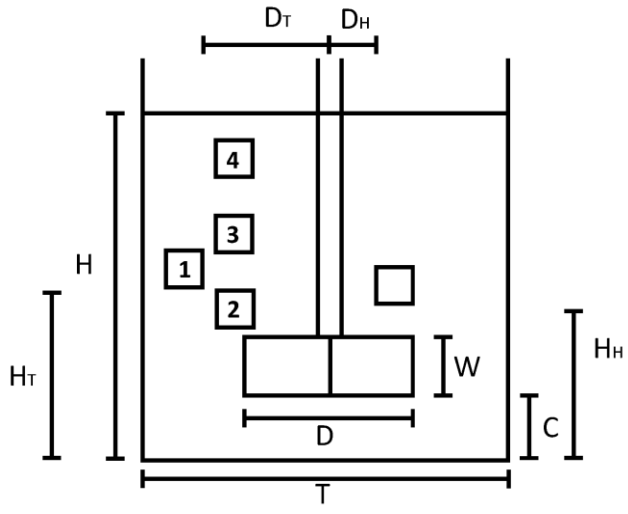

Part	Symbol	Dimension (mm)
Temperature sensor	$D_{T(1)}$	35
	$H_{T(1)}$	41
	$D_{T(2)}$	27
	$H_{T(2)}$	32
	$D_{T(3)}$	27
	$H_{T(3)}$	62
	$D_{T(4)}$	27
	$H_{T(4)}$	82
Heater	D_H	15
	H_H	32
Stirrer	D	46
	W	17
	C	15
Tank	T	99
	H	95

Figure 1. Reactor set-up heat pulse method in OptiMax.

The heat pulse method measures temperature profiles at different heights and widths in the reactor to study the influence of the location, as can be seen in Figure 1. The geometries of the probes are listed in Table 2.

Table 2. Geometries of the measurement and injection probe

Name	Method	Function	Diameter (mm)	Length (mm)	Specifications
Temperature sensor (Mettler Toledo)	Electrical heating Hot liquid injection	Measurement	8	150	Data collected every 2 s
Temperature sensor (OMEGA Engineering)	Electrical heating Hot liquid injection	Measurement	3	150	Data collected every 0.8 s
Heater (Mettler Toledo)	Electrical heating	Heat input	6	170	Power: 10 W Duration: 10 s
Tubing (Watson-Marlow)	Hot liquid injection	Heat input	5	150	Temp.: 32°C Duration: 10 s

Table 3 shows the solvent characteristics of the used solvents, which have an influence on heat mixing.

Table 3. Solvent characteristics and chemicals

Solvent	Company	Purity	Viscosity* (mPa s)	Density* (kg/m³)	Thermal conductivity* (W/(m K))	Heat capacity* (kJ/(kg K))
n-Pentanol	Sigma-Aldrich	99%	3.5	811	0.116	2.35
n-Octanol	Sigma-Aldrich	99%	7.4	824	0.134	2.33
Formic acid	Sigma-Aldrich	97%	2.0	1220	0.274	2.15
Propionic acid	Sigma-Aldrich	99.5%	1.0	988	0.147	2.14
Water	/	Ultrapure (Cond. ~ 0.055 µS/cm)	1.0	998	0.600	4.19
Aniline	Sigma-Aldrich	99.5%	3.8	1022	0.172	2.18
Formamide	Sigma-Aldrich	99.5%	3.3	1133	0.353	2.40
Ethylene glycol	Sigma-Aldrich	99%	16.0	1115	0.290	2.47
n-Pentane	Sigma-Aldrich	99%	0.24	626	0.113	2.34
n-Decanol	Sigma-Aldrich	98%	12.0	830	0.162	2.36
2-Octanol	Sigma-Aldrich	97%	6.2	821	0.144	2.53

*solvent characteristics at 20°C[43–46]

2.2 Temperature sensors

The standard reactor set-up for the experiments is visualized in Figure 1. Three Pt100 1/10 DIN (OMEGA Engineering™) and one Pt 100 DIN (Mettler Toledo) resistance temperature sensors measure the temperature profile in the reactor. The data collecting frequency of the three temperature sensors of OMEGA Engineering are limited to a measurement every 0.8, while the temperature sensor of Mettler Toledo is programmed to measure every 2 s.

2.3 Heat pulse

Heat input is performed by two different methods: by an electrical resistance heater or by a hot liquid injection. When the heat pulse method is performed electrically, the power of the electrical heating probe (calibration heater, Mettler Toledo) is used at a power of 10 W and pulse duration of 10 s.

The Harvard Apparatus (PhD 2000) syringe pump with 2.4 mm tubing (Watson-Marlow) injects 3 mL for 10 s to the reactor volume. The same solvent or mixture as is already in the reactor content is injected at a temperature of 32 °C, thus avoiding additional heat of mixing and solvent contamination. The injected power of the hot liquid injection is calculated with eq 5.

$$P = \dot{m} * c_p * \Delta T = Q_v * \rho * c_p * \Delta T \quad (5)$$

With P the power, ṁ the mass flow, ΔT the temperature difference between injection and reactor content and Q_v the volumetric flow. Since the volumetric flow and temperature difference between injection and solvent are kept constant, the power depends on the heat capacity and density, which are solvent characteristics. During these tests, the power of the hot liquid injection varies from 5 W (n-pentane) to 15 W (water).

2.4 Heat pulse method

Upon a changing temperature, a dynamic error between the actual temperature in the reactor and the output signal, the measured temperature by the sensor exists. This dynamic error is approached as a first order nonlinear system and compensated by eq 6[47–51]. The time constant of the sensor, shown in eq 7, characterizes the dynamic error[47,49,50]. A time constant of 1.1 s for the three Pt100's of OMEGA Engineering and a time constant of 4.0 s for the Pt100 of Mettler Toledo is practically determined by applying a temperature step and comparing the measured and actual temperature profile. Figure 2 shows the comparison for a Pt100 of OMEGA Engineering between an immediate temperature step, the measured temperature step and the compensated temperature step, using eq 6.

$$T_{real,2} = T_{meas,1} + \frac{T_{meas,2} - T_{meas,1}}{1 - e^{-\frac{t}{\tau}}} \quad (6)$$

$$\tau = \frac{m * c_p}{U * A} \quad (7)$$

With $T_{real,2}$ the real temperature at the second measurement, $T_{meas,2}$ the measured temperature at the second measurement, $T_{meas,1}$ the measured temperature at the first measurement, t the time difference between measurements, τ the time constant, m the mass of the measuring part of the temperature sensor, c_p the specific heat capacity of the measuring part of the temperature sensor and U and A the overall heat transfer coefficient and heat exchange area of the measuring part of the temperature sensor.

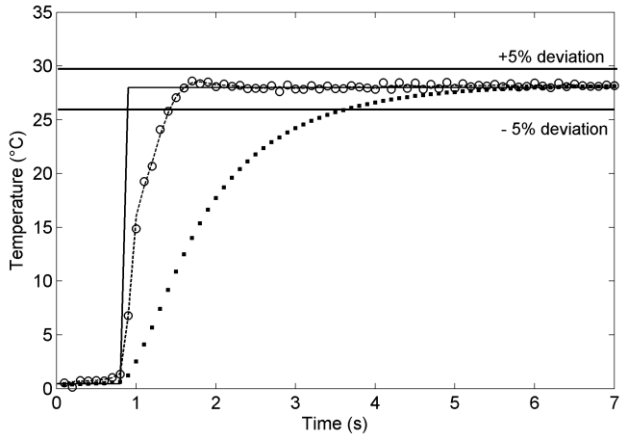

Figure 2. Comparison between immediate temperature step (—), measured temperature profile (■), corrected temperature profile (○) and smoothed temperature profile (– –).

The solid line shows the theoretical temperature change: when changing the temperature sensor from the ice bath to the hot water bath. The squared markers indicate the measured temperature profile. The sensor slowly adjusts to the new temperature due to the time constant of the sensor. It takes 3.0 s to reach the new temperature with a deviation of 5%. Eq 6 is used to compensate the dynamic error, which is represented by the round markers. The corrected temperature profile has a good match with the theoretical temperature profile. This correction reduces the error between the real and measured temperature, which results in a time of 0.7 s to reach the new temperature with a deviation of 5%. The corrected temperature profile thus provides a good approach for the temperature profile inside the reactor, however, the compensation of the dynamic error of the sensor results in an increase in noise on the measurements. The noise, which occurs at the constant temperatures before and after the temperature increase, is minimized by using a robust locally weighted scatterplot smoothing, Rloess[52,53]. Furthermore, smoothing enables the possibility to predict the temperature at every point in time, not only where a data point is provided[52–54]. Smoothing of the corrected temperature profile decreases the time to reach the new temperature with a deviation of 5% to 0.62 s.

The heat pulse experiment, shown in Figure 3, consists of a 10 s pulse of the electrical heater (solid line), which causes the temperature in the batch reactor to increase after distribution of the heat by the stirrer. The measured temperature profile is displayed by the squared markers, the corrected temperature profile by round markers and finally the data after correction and smoothening is represented by a dashed line.

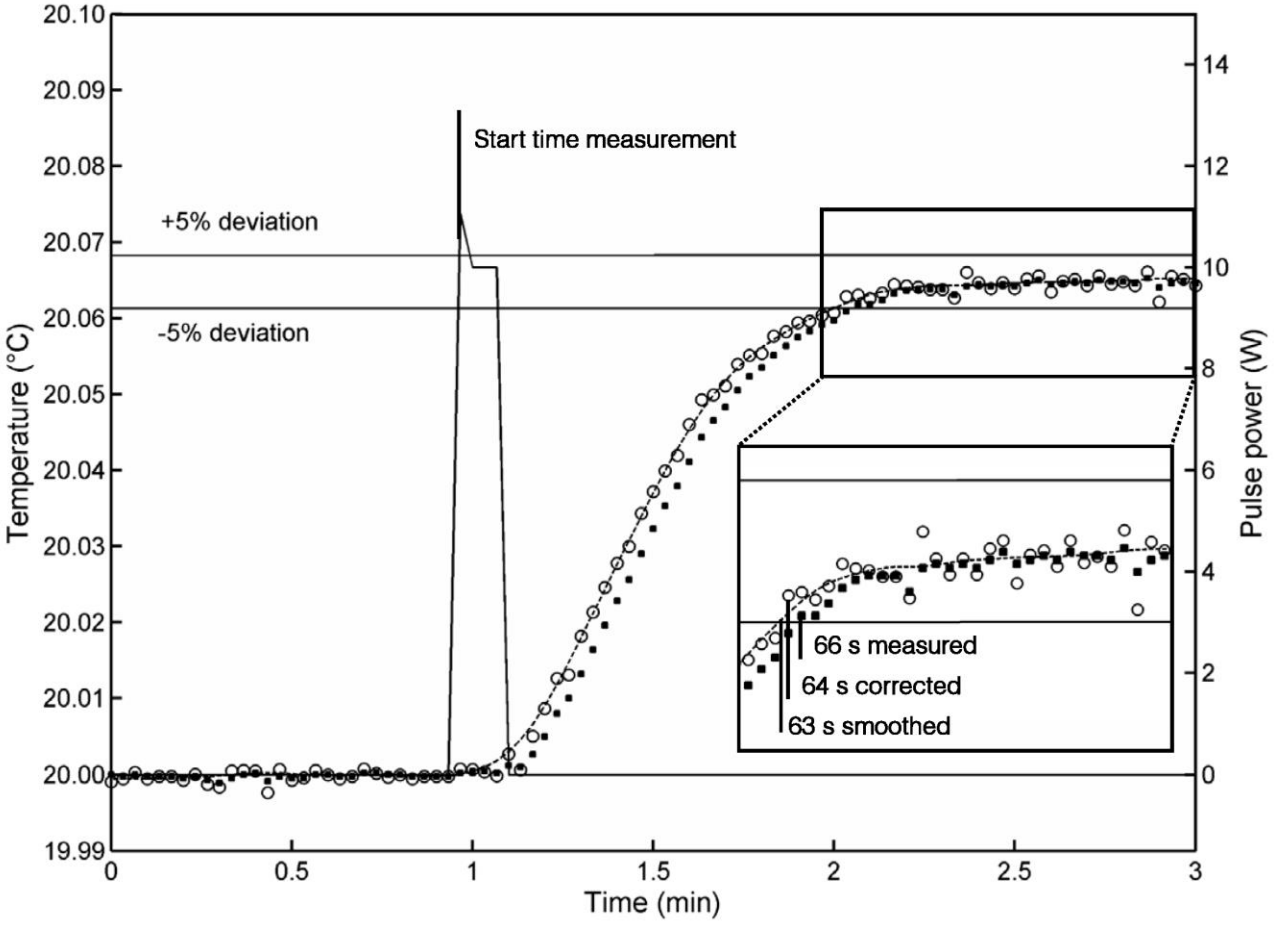

Figure 3. Temperature profiles of the heat pulse experiment at 50 RPM in pentane, with the pulse power visualized by the solid line (—) (right y-axis), the measured temperature profile (■), the corrected temperature profile (○) and the smoothed temperature profile (– –) versus temperature (left y-axis).

Each heat pulse experiment yields a characteristic temperature profile. The measured temperature starts with a constant temperature of 20.000 °C and a standard deviation on the measurement of +/- 0.0004 °C, calculated with 100 data points at 20.000 °C. The heat is mixed and distributed over the reactor content, which increases the reactor temperature. After the heat is homogeneously distributed, a new constant temperature is reached. The 95% mixing time is determined by the homogeneity criterion and is the time between the start of the heat pulse and the time to achieve a temperature, deviating 5% form the final temperature. For the measured temperature profile this amounts to 66 s. The corrected temperature profile has a 95% mixing time of 64 s. The correcting and smoothing of the temperature profile makes the method more universal: any temperature sensor can be used as long as the sensor is sensitive enough to measure the temperature increase and the time constant of the sensor is known to compensate the dynamic error of the sensor. In this research, two types of Pt100 are used, however, each sensor gives the same 95% mixing time by correcting and smoothing the data. In a minority of the performed heat pulse experiments, the increase in noise by the correction results in an increase in 95% mixing times. The smoothing of the corrected temperature profile reduces the noise and prevents errors in calculations of the 95% mixing time. For this experiments, the smoothing results in a 95% mixing time of 63 s, after the correction already is performed.

Every experiment of the heat pulse method is at least performed twice and the average 95% mixing time is used as data point. If this results in a large difference, more than two times the data collecting frequency, between the two 95% mixing times, a third test is performed to determine the average and standard deviation.

2.5 Local mixing factor

Mixing differs for each location in the reactor, which is compensated by the local mixing factor as specified in eq 2. By comparing the 95% mixing times of the different locations in the reactor with the average micromixing time, the local mixing factors are determined at each location. The local micromixing time in eq 3, which specifies mixing at a certain location, is calculated by multiplying the average micromixing time with the local mixing factor.

In addition, a validation of the local mixing factor is performed with CFD modelling in Comsol Multiphysics® 4.4. The rotating machinery mixer module of Comsol Multiphysics® 4.4 is used to determine the local mixing factor for each solvent and rotational speed. In the computations, the Reynolds-averaged-Navier-Stokes equations (RANS) are solved using the k-ε turbulence model[1]. The stationary solver uses Newton's method for solving a non-linear system of equations. A modelling solution is found when the relative tolerance is below 0.001 for the stationary solver of the RANS equations. Iterations to obtain the solution use a generalized minimal residual (GMRES) solver[55]. All solid surfaces function under no-slip boundary conditions. Tetrahedral meshes with a normal size provide results that are mesh independent.

2.6 Modelling software

Eureqa® (Nutonian), a non-linear statistical modeling software program, is used to create the model between heat and mass mixing. The fitting tool uses artificial programming to find a general equation that suits the data by producing generations of equations. The Pearson correlation coefficient is used as target statistical parameter[56,57].

3. Results and Discussion

3.1 Heat pulse method

The influence of the heat dosing parameters is investigated. Firstly, the power of the injection probe is varied from 5 to 20 W, where the pulse power has no influence, as long as isoperibolic conditions are achieved. With increasing pulse power, the final temperature increases, but the driving force gains as well, resulting in a constant 95% mixing time. Secondly, the pulse duration is varied from 5 to 20 s, where the pulse duration does have an influence on the 95% mixing time. A pulse with a longer duration causes a longer period of heat distribution throughout the reactor. For all experiments in this study, a heat pulse of 10 s is used. Thirdly, in figure 4, the two different heat pulse methods are compared.

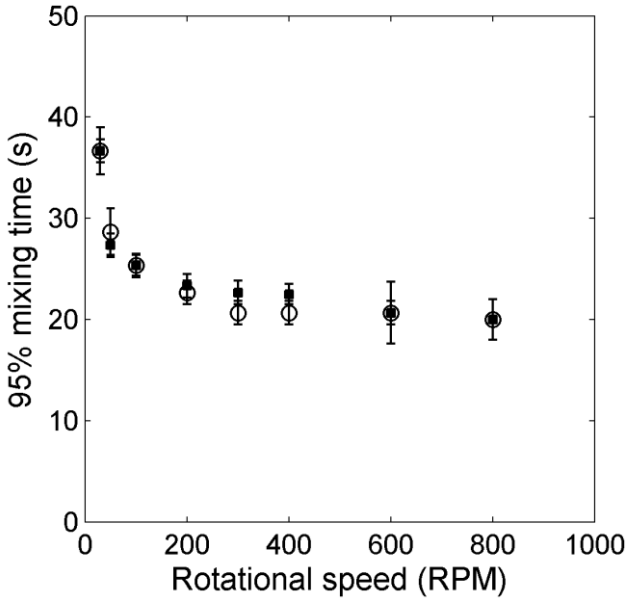

Figure 4. Comparison between the heat pulse methods, electrical resistance heating (○) and hot liquid injection (■) in water

Electrical heating and hot liquid injection both have an pulse duration of 10 s. However, the pulse powers of the two methods are 10 W and 15 W respectively. The two different methods to

add heat show a decrease in mixing time when the rotational speed increases, until a rotational speed of 300 RPM has been reached. From this point, the mixing time has reached a plateau and heat mixing cannot be further improved by increasing the rotational speed. This means that from this rotational speed conduction controls the homogenization of heat and therefore the mixing time cannot be further improved. The mixing times of the both methods show the same results, indicating that the same type of heat mixing is measured (in situ macromixing). This conformity also signifies that mesomixing by the injection of the liquid has a limited effect on heat mixing in this set-up.

In general, the heat pulse method using hot liquid injection is more flexible as the total amount of heat injected can be easily modified by changing the flow rate or the temperature of the hot liquid and is therefore also interesting to use at different scales.

The goal of the heat pulse method is to measure mass mixing in situ in a fast, robust way, without the destruction of the solvent. However, the 95% mixing time of the heat pulse method measures heat mixing in the reactor volume, not mass mixing. Therefore, a heat mixing model is needed that is able to eliminate the contribution of conduction on mixing and actually measures the local mass mixing. Figure 7 shows the influence of thermal conduction and local micromixing time on the 95% mixing time for four solvents: water, propionic acid, 2-octanol and ethylene glycol in water (50 wt %).

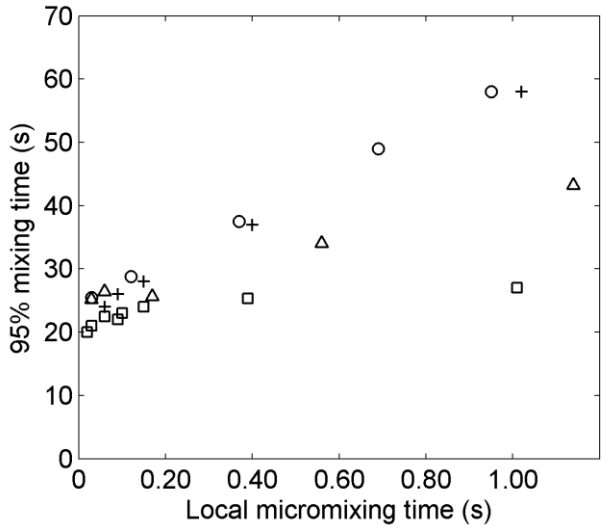

Figure 5. Relation between 95% mixing time and micromixing time of water (□), propionic acid (○), 2-octanol (+) and ethylene glycol in water (50 wt %) (Δ)

Water and propionic acid, respectively the square and round markers, have similar solvent characteristics except for the thermal diffusivity which is two times lower for propionic acid (6.93 * 10^{-8} m²/s) compared to water (14.4 * 10^{-8} m²/s). This results in much higher 95% mixing times for propionic acid at high local micromixing times. This indicates the influence of thermal conduction on mixing at a microscopic scale. At lower local micromixing times, where faster convection occurs, the differences in 95% mixing times decrease, due to the diminishing contribution of thermal conduction to the overall heat mixing.

Propionic acid and 2-octanol have similar solvent characteristics, except for the viscosity, where 2-octanol (7.55*10^{-6} m²/s) has a 7.5 times higher kinematic viscosity than propionic acid (1.03*10^{-6} m²/s). Since the micromixing time, eq 1, takes the kinematic viscosity into account, 95% micromixing times for propionic acid and 2-octanol are similar. The 95% mixing times of the solution of ethylene glycol in water (50 wt %) (triangle markers) is located between that of the organic solvents and water because the thermal diffusivity of 50% ethylene glycol – 50% water

($11.4*10^{-8}$ m²/s) is in between the thermal diffusivity of water ($14.4*10^{-8}$ m²/s) and propionic acid ($6.93*10^{-8}$ m²/s). The other solvent parameter of importance, kinematic viscosity, and reactor parameters, power number and rotational speed, are taken into account by local micromixing time. To conclude, Figure 5 shows that both thermal conduction and local micromixing time have a significant influence on the 95% mixing and that a model is needed to determine mass mixing by eliminating thermal conduction.

It is possible to perform the experiments at different reactor temperatures in order to take the influence of the temperature on solvent properties like density, thermal diffusivity and viscosity into account. This mimics reaction circumstances as closely as possible. However, in order to be able to accurately perform the heat pulse method at high temperatures, the reactor needs a jacket that guarantees a good insulation.

3.2 Heat mixing model

A heat mixing model is formulated by collecting 164 mixing times using 10 solvents with different solvent characteristics, varying the rotational speed and measuring the 95% mixing: times at 4 different locations. Eureqa® (Nutonian) is used to create the model and relates three heat mixing parameters. The first parameter is the 95% mixing times (θ_m), derived from the heat pulse experiments. The second parameter is the local micromixing time, calculated using eq 3 with the calculated average micromixing time and the local mixing factor. The experimentally determined local mixing factors are constant at one location and have errors below 25% compared to the CFD modelled local mixing factors. Table 4 compares experimental and modelled local mixing factors for both water and 2-octanol at all four locations, visualized in figure 1.

Table 4. Comparison local mixing factors experimental and CFD for water and 2-octanol

	WATER		2-OCTANOL	
Method	CFD	EXPERIMENTAL	CFD	EXPERIMENTAL
Location 1	1.4	1.5	1.4	1.5
Location 2	2.4	2.8	2.4	2.1
Location 3	0.9	0.8	0.7	0.8
Location 4	0.4	0.4	0.3	0.4

At location 1 and 2, CFD values are the same for the two solvents and have a difference of below 20% compared to the experimental values. At location 4, which is located further away from the stirrer, the modelled local mixing factor is influenced by the higher viscosity of 2-octanol compared to water. This causes the stirrer energy to be more concentrated around the stirrer and therefore decreases the local mixing factor at location 4.

The third parameter is the thermal diffusivity, which is a solvent dependent constant, calculated with eq 4. Table 5 summarizes the parameter ranges, while eq 8 shows the heat mixing model for the 1 L reactor with a filling degree of 80%. It should be noted that the model is dimensionally inconsistent.

$$\theta_m = 25.6 - 0.314 * 10^8 * \alpha + (59.2 - 3.55 * 10^8 * \alpha) * t_{m,local} \quad (8)$$

Table 5. Model parameter ranges

Parameter	Symbol	Parameter range	unit
Rotational speed	N	$30 - 1200$	min^{-1}
Local micromixing time	$t_{m,local}$	$1.200 - 0.011$	s
Dynamic viscosity	μ	$0.24 - 12.0$	$mPa.s$

Density	P	$626 - 1133$	$\frac{\mathrm{kg}}{\mathrm{m}^3}$
Thermal diffusivity	A	$6.05 * 10^{-8} - 14.4 * 10^{-8}$	$\frac{\mathrm{m}^2}{\mathrm{s}}$
Local mixing factor	f_{local}	$0.3 - 2.4$	/

Heat mixing, characterized by the 95% mixing time, involves two mechanisms: convection, characterized by local micromixing time, and conduction, characterized by thermal diffusivity. The mechanisms are separated using eq 8 in order to measure mass mixing using the heat pulse method. However, since the model uses local micromixing as a characteristic mass mixing value, the model is only valid for convection by engulfment. Engulfment as dominating mixing mechanism takes place for solvents with a Schmidt number below 4000. Solvents with Schmidt numbers much higher than 4000 differ from the model due to deviations in the mixing mechanism, since diffusion can no longer be neglected and the Engulfment-Deformation-Diffusion (EDD-model) becomes relevant[1,8,17].

The heat mixing model, eq 8, consists of four terms, which can be explained by two different influences:

- The first two terms describe the 95% mixing at the lowest micromixing times, thus at the highest rotational speeds. These terms mean that at infinite mixing, the lowest possible 95% mixing time that can be reached depends on thermal conduction (α). This implicates that mixing of heat will always need thermal conduction to mix to the microscopic scale;
- The third and fourth term correspond to the influence on the 95% mixing time of thermal convection and thermal conduction, respectively. The local micromixing time has a linear relation with the 95% mixing time, however, the slope depends on thermal

conduction. A high thermal diffusivity of the solvent increases the distribution of heat and therefore decreases the slope of the trend, resulting in lower 95% mixing times.

This heat mixing model enables the possibility to quantify mixing times and to compare mass mixing in different solvents and non-reactive mixtures with Schmidt numbers below 4000. The use of this heat mixing model separates the effect of thermal conduction and thermal convection on the 95% mixing time. The heat mixing model makes the heat pulse method capable of measuring mass mixing at any location, except close to the liquid surface, where heat exchange processes occur which decrease the accuracy of the method. The heat pulse method can be used in three ways:

1. The heat pulse method can be used to measure optimal mixing and homogeneity of mixing in the reactor volume by varying the rotational speed and measuring the 95% mixing time at multiple locations. At a certain rotational speed, optimal mixing is achieved, all sensors indicate the same lowest 95% mixing time and mixing can no longer be improved;
2. The model can translate 95% mixing times of the heat pulse method to local micromixing time and compare mass mixing at a location of interest to the average micromixing time in order to know the local mixing factor for a solvent or non-reactive mixture of interest;
3. The model can predict mass mixing for a new solvent or reactive mixture. For example, the heat mixing model can be used to predict 95% mixing times at different locations and rotational speeds. These predicted values then indicate where homogeneous mass mixing occurs and where mass mixing can no longer be improved.

Not only the meaning and application of the heat mixing model are important, the ability to accurately predict heat mixing in the reactor is of great importance as well. Therefore, the

statistical match between model and experiments are shown in Figure 6, where the linearity between the predicted and practical values of the 95% mixing times is expressed as well.

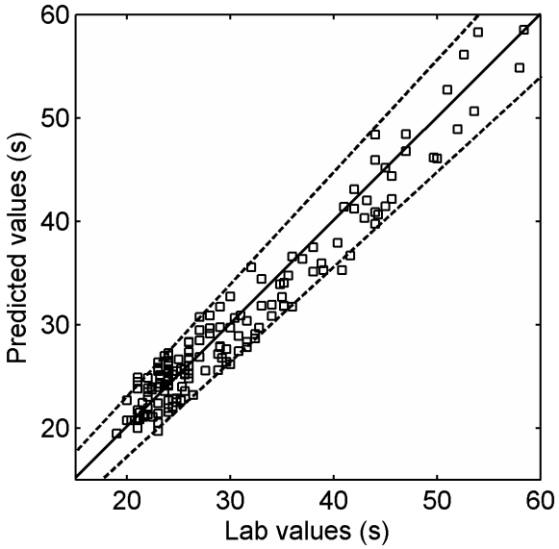

Substance	Value
R^2	0.943
Correlation coefficient	0.972
Maximum error	7.3 s
Mean squared error	4.7 s
Mean absolute error	1.7 s

Figure 6. Linear relation between the predicted and practical values with a 10% error margin (- -) and statistical values of the model

A good match exists between the predicted and practical 95% mixing times, resulting in a linear relationship. The majority of the values lay within the 10% error margin. To further visualize the match between practical and predicted results, figure 7 shows the lab (markers) and predicted (lines) values for water, propionic acid, 2-octanol and ethylene glycol in water (50 wt %) for local micromixing times.

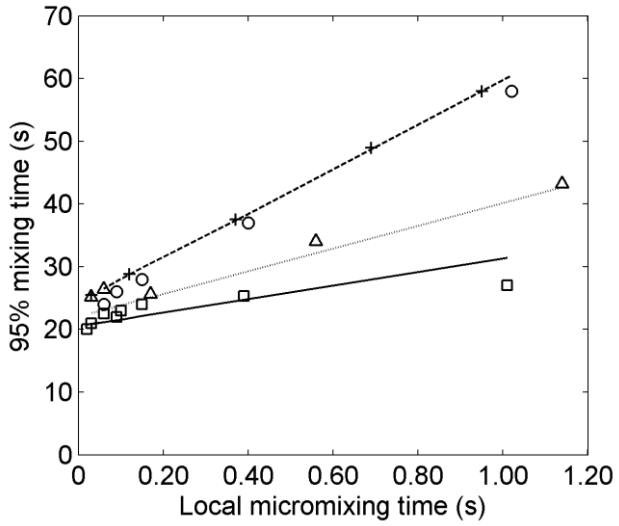

Figure 7. Comparison between predicted mixing times of water (—), propionic acid and 2-octanol (– –) and ethylene glycol in water (50 wt %) (···) and the measured mixing times of water (□), propionic acid (○), 2-octanol (+) and ethylene glycol in water (50 wt %) (Δ)

Despite the high coefficient of determination, there are still some deviations between the model and the lab values. The deviations on the experimental 95% mixing times are also due to the limited data collecting frequency of 0.8 s to 2 s, depending on the used data acquisition module, which limits the sensitivity of the method. The correcting and smoothing of the data are able to improve the sensitivity, however, this cannot prevent experimental errors between lab and predicted results.

Highly thermal conductive solvents have a flatter slope of the regression curve which decreases the accuracy of the method. When using the model to translate the 95% mixing time to local micromixing time, the limitation in sensitivity by the data collecting frequency causes deviations on the calculated local micromixing times as well. These deviations are larger for highly conductive solvents due to the flatter slope. For example, the error due to the limited data collecting frequency at a local micromixing time of 1.0 s for propionic acid, a low thermal conductive solvent, is 6.5%, while the deviation for water, a high thermal conductive solvent, is 22%.

Figure 7 visualizes the match between model and experimental data, used to create the model. When comparing the model with a solvent that is excluded to create the model, n-pentanol, a standard error of 8% occurs.

4. Conclusion

A new method that is capable of measuring local mass mixing, is developed for 800 mL liquid in a 1 L batch reactor with a 4 PBT with an angle of 45°. The method consists of an injection of a heat pulse, measuring the temperature increase under isoperibolic conditions with temperature sensors positioned at different locations. The heat pulse is defined by a duration of 10 s with a power of 5 to 15 W. After correction of the dynamic error, the temperature profile of a PT100 is smoothed with Rloess and used to calculate the 95% mixing time. Using the lab data of the heat pulse method, a heat mixing model is developed that identifies the effects of thermal conduction and convection at heat mixing.

The heat pulse method has three important functions. Firstly, it measures optimal mixing and mixing homogeneity in the reactor volume. Secondly, the model of the heat pulse method calculates local micromixing at the location of interest. Finally, the model is able to predict mass mixing in the reactor for new solvents or reaction mixtures. The heat pulse method can be with non-reactive mixtures at room or reaction temperature. It can be rapidly performed multiple times without destroying the solvent, since it only adds heat or a small quantity of liquid to the volume.

In this study, the versatility and applicability of the heat pulse method is demonstrated. In future work, the heat pulse method will be validated and benchmarked against existing mass mixing characterization. Furthermore, the applicability of the heat pulse method on different reactor sizes will be investigated.

AUTHOR INFORMATION

Corresponding Author

*E-mail: Lennart.camps@kuleuven.be; Leen.thomassen@kuleuven.be

ACKNOWLEDGMENT

This work is made possible by Mettler Toledo and Janssen Pharmaceutica, part of Johnson & Johnson. The authors gratefully acknowledge the financial support of the KU Leuven Impulsfonds IMP/16/023.

ABBREVIATIONS

A, contact area, m^2; c_p, specific heat capacity, kJ/(kg*K); D, diameter of the stirrer, m; f_{local}, local mixing factor, dimensionless; k, thermal conductivity, W/(m*K); m, mass of measuring part of temperature sensor, kg; $\dot{m}$, mass flow, kg/s; P, power, W; n_p, power number, dimensionless; $Q_{v,}$ the volumetric flow, m^3/s; t, time difference between measurements, s; $t_{m,ave}$, average micromixing time, s; $t_{m,local}$, local micromixing time, s; $T_{meas,1}$, measured temperature at the first time frame, °C; $T_{meas,2}$, measured temperature at the second time frame, °C; $T_{Real,2}$, real temperature at the second time frame, °C; ΔT, temperature difference between injection and reactor content, °C; U, overall heat transfer coefficient, $W/(m^2 K)$; V, reactor volume, m^3.

α, thermal diffusivity, m^2/s; ε_{ave}, average energy dissipation, W/kg; ε_{local}, local energy dissipation, W/kg; θ_m, 95% mixing time, s; μ, dynamic viscosity, Pa s; ρ, density, kg/m^3; ν, kinematic viscosity, m^2/s; τ, time constant, s.

REFERENCES

(1) Paul, E. L.; Atiemo-Obeng, V. A.; Kresta, S. M. *Handbook of Industrial Mixing. Science and Practice*; 2004.

(2) Perry, R.; Green, D.; Maloney, J. *Perry's Chemical Engineers' Handbook*; 1997.

(3) Simard, M. Scaleup Options and Risk to Commercial Scale. **2011**, No. 1.

(4) Schwolow, S.; Heikenwälder, B.; Abahmane, L.; Kockmann, N.; Röder, T. Kinetic and Scale-up Investigations of a Michael Addition in Microreactors. *Org. Process Res. Dev.* **2014**, *18* (11), 1535–1544.

(5) Klaewkla, R.; Arend, M.; Hoelderich, W. F. A Review of Mass Transfer Controlling the Reaction Rate in Heterogeneous Catalytic Systems. *Mass Transf. - Adv. Asp.* **2011**, No. 3, 667–684.

(6) Stoker, E. B. Comparative Studies on Scale-Up Methods of Single-Use Bioreactors By. **2011**.

(7) Deans, S.; Fitzgerald, M. Techniques for Mixing and Scaling in Mechanically Agitated Vessels. **2017**, 69.

(8) BALDYGA, J. .; Pohorecki, R. Turbulent Micromixing in Chemical Reactors - a Review. *Chem. Eng. J.* **1995**, *58* (2), 183.

(9) Belle, C. Van. Koppelen van Transportfenomenen En Intrinsieke Kinetiek Voor Vrije Radicalaire Polymerisatieprocessen . **2009**.

(10) Akiti, O. Turbulent Mixing And Chemical Reaction In Baffled Stirred Tank Reactors: A

Comparison Between Experiments And A Novel Micromixing-Based Computational Fluid Dynamics Model. *Public Health* **2007**, 125.

(11) Al-hengari, S. Process Intensification : A Study of Micromixing and Residence Time Distribution Characteristics in the Spinning Disc Reactor. **2011**, No. October.

(12) Tunestål, E. Investigations of Micromixing - In Alfa Laval's Art Plate® Reactors. **2012**, 66.

(13) Baldyga, J.; Bourne, J. R. Interactions between Mixing on Various Scales in Stirred Tank Reactors. *Chem. Eng. Sci.* **1992**, *47* (8), 1839–1848.

(14) BALDYGA, J. ;BOURNE J. R. Simplification of Micromixing Calculations. I. Derivation and Application Of. **1989**, *42*, 83–92.

(15) Bamps, B. INVESTIGATION OF MICROMIXING IN AN ULTRASOUND BATCH REACTOR. **2015**, 1–99.

(16) Furukawa, H.; Kato, Y.; Inoue, Y.; Kato, T.; Tada, Y.; Hashimoto, S. Correlation of Power Consumption for Several Kinds of Mixing Impellers. *Int. J. Chem. Eng.* **2012**, *2012*.

(17) Baldyga, J.; Bourne, J. R. Comparison of the Engulfment and the Interaction-by-Exchange-with-the-Mean Micromixing Models. *Chem. Eng. J.* **1990**, *45*, 25–31.

(18) Tzou, D. Y. Macro- to Microscale Heat Transfer. *Macro- to Microscale Heat Transf. Lagging Behav. Second Ed.* **2014**, 1–552.

(19) Lienhard, J. H. A Heat Transfer Textbook. *J. Heat Transfer* **2010**, *82* (1), 198.

(20) Incropera, F. P.; Bergman, T. L.; Lavine, A. S.; DeWitt, D. P. *Fundamentals of Heat and Mass Transfer*; 2011.

(21) Vlachopoulos, J.; Strutt, D. Asic Heat Transfer and Some Applications in Polymer Processing. *Plast. Tech. Toolbox* **2002**, *2*, 21–33.

(22) Cabaret, F.; Bonnot, S.; Fradette, L.; Tanguy, P. A. Mixing Time Analysis Using Colorimetric Methods and Image Processing. *Ind. Eng. Chem. Res.* **2007**, *46* (14), 5032–5042.

(23) Sardeshpande, M. V.; Kumar, G.; Aditya, T.; Ranade, V. V. Mixing Studies in Unbaffled Stirred Tank Reactor Using Electrical Resistance Tomography. *Flow Meas. Instrum.* **2016**, *47* (October), 110–121.

(24) Kuzmanić, N.; Ljubičić, B. Suspension of Floating Solids with Up-Pumping Pitched Blade Impellers; Mixing Time and Power Characteristics. *Chem. Eng. J.* **2001**, *84* (3), 325–333.

(25) Rousseaux, J.-M.; Muhr, H.; Plasari, E. Mixing and Micromixing Times in the Forced Vortex Region of Unbaffled Mixing Devices. *Can. J. Chem. Eng.* **2001**, *79* (5), 697–707.

(26) Bonvillani, P.; Ferrari, M. P.; Ducrós, E. M.; Orejas, J. A. Theoretical and Experimental Study of the Effects of Scale-up on Mixing Time for a Stirred-Tank Bioreactor. *Brazilian J. Chem. Eng.* **2006**, *23* (1), 1–7.

(27) Post, T. Understand the Real World of Mixing. *Chem. Eng. Prog.* **2010**, *106* (3), 25–32.

(28) Ascanio, G. Mixing Time in Stirred Vessels: A Review of Experimental Techniques. *Chinese J. Chem. Eng.* **2015**, *23* (7), 1065–1076.

(29) Nere, N. K.; Patwardhan, A. W.; Joshi, J. B. Liquid-Phase Mixing in Stirred Vessels : Turbulent Flow Regime. **2003**, 2661–2698.

(30) Guichardon, P.; Falk, L. Characterisation of Micromixing Efficiency by the Iodide - Iodate Reaction System . Part I: Experimental Procedure. *Chem. Eng. Sci.* **2000**, *55*, 4233–4243.

(31) Guichardon, P.; Falk, L.; Villermaux, J. Characterization of Micromixing Efficiency by the Iodide-Iodate Reaction System. Part II: Kinetic Study. *Chem. Eng. Sci.* **2000**, *55* (19), 4245–4253.

(32) Guichardon, P.; Falk, L.; Andrieu, M. Experimental Comparison of the Iodide-Iodate and the Diazo Coupling Micromixing Test Reactions in Stirred Reactors. *Chem. Eng. Res. Des.* **2001**, *79* (8), 906–914.

(33) Kozicki, F.; Bourne, J. R. MLXING AND FAST CHEMICAL - L. **1981**, *36* (Id), 1643–1648.

(34) Min, J.; Gao, Z. Large Eddy Simulations of Mixing Time in a Stirred Tank. *Chinese J. Chem. Eng.* **2006**, *14* (1), 1–7.

(35) Behle, M.; Schulz, K.; Leiner, W.; Fiebig, M. Color-Based Image Processing to Measure Local Temperature Distributions by Wide-Band Liquid. *Appl. Sci. Res.* **1996**, *56*, 113–143.

(36) Fournier, M.-C.; Falk, L.; Villermaux, J. A New Parallel Competing Reaction System for Assessing Micromixing Efficiency—Experimental Approach. *Pergamon Chem. Eng. Sci.* **1996**, *51* (22), 5053–5064.

(37) Malvern Ltd. A Basic Guide to Particle Characterization. **2015**.

(38) Kumaresan, T.; Joshi, J. B. Effect of Impeller Design on the Flow Pattern and Mixing in Stirred Tanks. *Chem. Eng. J.* **2006**, *115* (3), 173–193.

(39) Assirelli, M.; Bujalski, W.; Eaglesham, A.; Nienow, A. W. Macro- and Micromixing Studies in an Unbaffled Vessel Agitated by a Rushton Turbine. *Chem. Eng. Sci.* **2008**, *63* (1), 35–46.

(40) Gesthuisen, R.; Krämer, S.; Niggemann, G.; Leiza, J. R.; Asua, J. M. Determining the Best Reaction Calorimetry Technique: Theoretical Development. *Comput. Chem. Eng.* **2005**, *29* (2), 349–365.

(41) Wilhelm, H.; Lühmann, T.; Rus, T.; Steglich, F. A Compensated Heat-Pulse Calorimeter for Low Temperatures. *Rev. Sci. Instrum.* **2004**, *75* (8), 2700–2705.

(42) Richner, G.; Neuhold, Y. M.; Papadokonstantakis, S.; Hungerbühler, K. Temperature Oscillation Calorimetry for the Determination of the Heat Capacity in a Small-Scale Reactor. *Chem. Eng. Sci.* **2008**, *63* (14), 3755–3765.

(43) Kauffman, G. W.; Jurs, P. C. Prediction of Surface Tension, Viscosity, and Thermal Conductivity for Common Organic Solvents Using Quantitative Structure-Property Relationships. *J. Chem. Inf. Comput. Sci.* **2001**, *41* (2), 408–418.

(44) MEGlobal. Ethylene Glycol Product Guide. *Comp. Gen. Pharmacol.*

(45) Pinot, J.; Commenge, J. M.; Portha, J. F.; Falk, L. New Protocol of the Villermaux-Dushman Reaction System to Characterize Micromixing Effect in Viscous Media. *Chem. Eng. Sci.* **2014**, *118*, 94–101.

(46) Marcus, Y. *The Properties of Solvents*; 2003.

(47) Sarnes, B.; Schrüfer, E. Determination of the Time Behaviour of Thermocouples for Sensor Speedup and Medium Supervision. **2007**, *2*, 295–309.

(48) Acromag. Criteria for Temperature Sensor Selection of T/C and Rtd Sensor Types. **2011**, No. May, 1–14.

(49) Zimmerschied, R.; Isermann, R. Nonlinear Time Constant Estimation and Dynamic Compensation of Temperature Sensors. *Control Eng. Pract.* **2010**, *18* (3), 300–310.

(50) Wang, Y. The Research of a New Type of Sensor Dynamic Compensation Technology d ω. **2011**, *15* (86), 1575–1579.

(51) Hung, P. C. F.; McLoone, S.; Irwin, G.; Kee, R. Unbiased Thermocouple Sensor Characterisation in Variable Flow Environments. *IFAC* **2015**.

(52) Cleveland, W.; Loader, C. Statistical Theory and Computational Aspects of Smoothing. *Stat. Theory Comput. Asp. Smoothing* **1996**, 10–49.

(53) Cleveland, W. S.; Devlin, S. J.; Grosse, E. Regression by Local Fitting. Methods, Properties, and Computational Algorithms. *J. Econom.* **1988**, *37* (1), 87–114.

(54) Nurunnabi, a.; West, G.; Belton, D. Robust Locally Weighted Regression For Ground Surface Extraction In Mobile Laser Scanning 3D Data. *ISPRS Ann. Photogramm. Remote Sens. Spat. Inf. Sci.* **2013**, *II-5/W2* (November), 217–222.

(55) Ayachour, E. H. A Fast Implementation for GMRES Method. *J. Comput. Appl. Math.* **2003**, *159* (2), 269–283.

(56) Wieland, R.; Rogasik, H. Method for Analyzing Soil Structure According to the Size of Structural Elements. *Comput. Geosci.* **2015**, *75*, 96–102.

(57) Chen, C.; Luo, C.; Jiang, Z. A Multilevel Block Building Algorithm for Fast Modeling

Generalized Separable Systems. *Expert Syst. Appl.* **2018**, *109*, 25–34.

GRAPHIC TABLE OF CONTENT

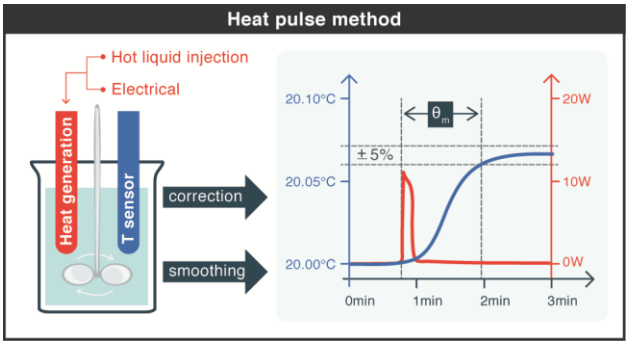

HIGHLIGHTS

1. Method is developed to measure heat mixing by injecting a short heat pulse
2. Heat mixing is related to mass mixing by a model for a 1 L reactor
3. Both convection and conduction are crucial in heat mixing
4. The model is able to predict mixing in the reactor for new solvents or reaction mixtures.

REFEREES

1. Thybaut, J. (Faculty of Engineering and Architecture, UGent, Belgium): Joris.Thybaut@UGent.be
2. Rousseaux, J. (CNRS - Ecole Nationale Superieure des Industries Chimiques INPL, Nancy Cedex, France): Jean-Marc-ROUSSEAUX@pechiney.com

3. Ascanio, G. (Center of Applied Sciences and Technological Development, National Autonomous University of Mexico, Ciudad Universitaria, Mexico): gabriel.ascanio@ccadet.unam.mx

4. Joshi, J. B. (Institute of Chemical Technology, University of Mumbai, Mumabi, India): jbj@udct.org